RESEARCH ARTICLE

MATERIALS SCIENCE

Engineering durable interphases for high-voltage Li-ion batteries under thermal stress

Shiming Chen[1,#], Wenguang Zhao[1,#], Guorui Zheng[2,*], Chenyu Yang[3], Taowen Chen[1], Hengyu Ren[1], Yue Zuo[1], Xiangming Yao[1], Ke Li[1], Haoyu Xue[1], Jianjun Fang[1], Yuxiang Huang[4], Kai Yang[5], Zu-Wei Yin[6], Luyi Yang[1,*] and Feng Pan[1,*]

[1]School of Advanced Materials, Peking University Shenzhen Graduate School, Shenzhen 518055, China;
[2]Institute of Materials Research (IMR), Tsinghua Shenzhen International Graduate School, Tsinghua University, Shenzhen 518055, China;
[3]National Synchrotron Radiation Laboratory, University of Science and Technology of China, Hefei 230029, China;
[4]Department of Chemistry, University of Hong Kong, Hong Kong 999077, China;
[5]Advanced Technology Institute, University of Surrey, Guildford GU2 7XH, UK;
[6]College of Energy, Xiamen University, Xiamen 361005, China
[#]Equally contributed to this work.
***Correspondence authors**. E-mails: zhengguorui1991@163.com; yangly@pkusz.edu.cn; panfeng@pkusz.edu.cn

ABSTRACT

Achieving stable cycling of high-voltage cathodes at elevated temperatures remains a critical challenge due to intensified interfacial side reactions and the accelerated dissolution of the cathode electrolyte interphase (CEI). In this work, based on theoretical calculations, Li_2SO_3 with desirable thermal stability and adhesiveness is proposed as a thermally stable binding agent between the selected CEI components (LiF and Li_3PO_4, where Li_3PO_4 facilitates fast Li^+ transport and thermal stability, while LiF serves as a stable, electron-blocking framework) to prevent undesirable dissolution. This is achieved by leveraging electrolyte engineering to modulate the solvation environment and promoting the in-situ formation of the aforementioned CEI architecture. Owing to its structural and compositional stability at elevated temperatures, the constructed CEI effectively

mitigates interfacial side reactions even under elevated temperature conditions. As a result, the uncommon achievement of stable cycling for $LiCoO_2$ at 4.6 V and 45°C was realized, demonstrating 81.9% capacity retention over 500 cycles. This work provides a transformative pathway for designing a durable CEI layer tailored to high-voltage and elevated temperature applications, paving the way for lithium-ion batteries to operate reliably in extreme environments.

Keywords: $LiCoO_2$ cathode, cathode electrolyte interphase, high-voltage and elevated temperature, electrolyte design strategy

INTRODUCTION

Driven by the ever-increasing demand for high energy density in portable electronic devices and electric vehicles, there is a growing need for advanced cathode materials in lithium-ion batteries (LIBs) that can be cycled stably at high cutoff voltages while delivering large specific capacities [1,2]. However, extending the operating voltage beyond 4.5 V vs Li/Li^+ poses significant challenges, including severe side reactions and irreversible phase transitions. Commercially used carbonate-based solvents are considered to form a non-uniform cathode electrolyte interphase (CEI), which is mainly composed of organic species with limited oxidative stability [3,4]. To stabilize the cathode interphase under high-voltage (HV) condition, an effective strategy is to modify the electrolyte to construct a CEI layer with desirable physicochemical properties [5]. For instance, the introduction of lithium difluoro(oxalato)borate contributes to construct a lithium fluoride (LiF)-rich interphase [6,7], which has been considered as an ideal inorganic component due to its chemical inertness, high Young's modulus and low electronic conductivity [8], thus suppressing the degradation of cathode. Besides, suitable ion conductor such as lithium phosphate (Li_3PO_4, $\sim 10^{-6}$ S cm^{-1}) is proved to reduce the redox activity for interfacial oxygen anions and suppress transition metal (TM) ion dissolution, enhancing the stability of cathode effectively [9,10].

Although the aforementioned efforts have successfully developed stable CEI layers on the cathode surface under HV condition, few studies have simultaneously addressed cycling stability at elevated temperatures, which is a critical safety metric for commercial LIBs [11]. Under such harsh conditions, cathodes would suffer more severe interfacial issues, including excess electrolyte decomposition and CEI dissolution [12,13]. The organic species in CEI layer tend to dissolve in the electrolyte at elevated temperature due to the lack of thermal stability, resulting in the dense CEI

structure at room temperature to be destroyed [14–16]. In this case, alternative CEI components needs to be introduced, which not only exhibits a wide bandgap and high thermal stability, but also features robust adhesion interaction with coexisting inorganic components, maintaining the structural integrity of CEI layer. In previous studies, the cycling stability of cathodes under elevated temperature condition have not received much attention as room [16,17]. Considering the diverse application scenarios and safety requirements of LIBs, it is crucial to regulate the electrolyte composition and solvation structure and construct a stable CEI structure under such harsh conditions.

Herein, the essential physiochemical properties of inorganics in CEI required to perform effectively under extreme conditions were outlined, including band gap, ionic conductivity, thermal stability and adhesive force. Therefore, we propose a multiple inorganics strategy for the design for CEIs under harsh conditions, where Li_3PO_4 facilitates fast Li^+ transport and high thermal stability, while lithium sulfite (Li_2SO_3) provides the necessary adhesiveness and LiF serves as a stable framework. Through introducing triethyl phosphate (TEP) and 1,3-propane sultone (PS) into the electrolyte, a trilayered CEI composed of Li_3PO_4, LiF, and Li_2SO_3 was constructed on the lithium cobalt oxide ($LiCoO_2$, LCO) cathode, which exhibiting high chemical-electrochemical stability and excellent anchoring strength. The designed CEI layer could effectively suppress surface degradation of LCO and restrain detrimental side reactions under harsh testing conditions (4.6 V at 45°C). Benefitting from the construction of robust CEI on cathode surface, high capacity and excellent cycling stability have been achieved, significantly outperforming traditional carbonate-based electrolytes.

RESULTS AND DISCUSSION

Design principles and physicochemical properties of electrolytes

As shown in **Figure 1a**, although LiF, as a major component of the CEI, has a relatively wide electrochemical window, its properties do not meet the aforementioned requirements in other aspects. During deep de-lithiation process, LCO cathode tends to suffer the escape of active oxygen species and the release of low-valence TM ions to maintain charge balance on the surface [18]. This process disrupts the CEI layers and exacerbates interface reactions. It is efficient to lower the O *2p* band center of LCO cathode, thereby improving the structural and interfacial stability [19]. Combing with the results of partial density of states (PDOS) for de-lithiated LCO cathodes, the role of various

anions (F^-, PO_4^{3-} and SO_3^{2-}) in enhancing interfacial oxygen stability at the atomic level are revealed (**Figure 1b** and **Figure S1**). Compared with pristine LCO cathode, both PO_4^{3-} and SO_3^{2-} reduce the O 2p band center position (-2.12 eV for LCO-PO_4 and -1.71 eV for LCO-SO_3), indicating a significant suppression of redox activity for oxygen anions.

Furthermore, to preserve the CEI integrity under elevated temperature conditions, the newly incorporated species should feature excellent thermal resilience and robust adhesion with coexisting interphase components. The thermal stability of various CEI components was evaluated by density functional theory (DFT) calculation and ab initio molecular dynamics (AIMD) simulation. Li_3PO_4 shows the largest cohesive energy (indicating the degree of interaction and bond strength in the interior of material) due to the robust P-O tetrahedron groups (**Figure S2**). The temperature curves of LiF, Li_3PO_4 and Li_2SO_3 obtained from AIMD simulation show that Li_2SO_3 also has the excellent thermal stability (**Figure 1c**).

Next, the adhesive force of inorganics was calculated, including the binding energies between LCO surface (**Figure S3**) and CEI components, and interfacial binding energies for interior CEI layer (**Figure 1d** and **Figure S4**). It is clear that Li_2SO_3 exhibits the highest adhesive force, serving as a binding agent in the CEI layer and contributing to prevent CEI from dissolution. Furthermore, the interaction force between heterogeneous inorganics would stretch the Li-anion bonds [20] and reduce the transport energy barrier of Li^+, thus further facilitating fast Li^+ conduction within CEI (**Figure S5**). Therefore, we propose a multi-inorganic strategy for CEI design under harsh conditions, comprising Li_3PO_4, LiF, and Li_2SO_3. In this structure, Li_2SO_3 provides vital adhesiveness and works synergistically with Li_3PO_4 to enhance the thermal stability and ionic conductivity of CEI layer, while LiF serves as a chemically stable and electron-blocking framework.

The designed electrolyte (denoted as FEDTP) is composed of 1.0 M $LiPF_6$ in fluoroethylene carbonate (FEC), ethyl methyl carbonate (EMC), diethyl carbonate (DEC) and TEP with a volume ratio of 2:4:3:1, which includes 1 vol% PS. For comparison, the electrolyte without adding PS (denoted as FEDT), the electrolyte without adding PS and TEP (denoted as FED) and the baseline carbonate electrolyte (denoted as EED, more detail information can be found in **Supporting Information**) were also prepared. At 45°C, LCO cathode suffered a dramatic capacity loss in EED due to the unstable electrolyte and radical interface reaction (**Figure S6**). In this view, EC solvent is replaced with FEC, which exhibits better oxidative stability. The linear sweep voltammetry (LSV)

curves show that the FEDTP system shows an early oxidation peak, corresponding to the formation of CEI (**Figure S7**), which is consistent with the theoretical results (**Figure 2a**). Besides, it has been reported that the autocatalytic decomposition of $LiPF_6$ under elevated temperature leads to the formation of PF_5, which would react with trace amount water to form HF, resulting in severe damage of CEI and battery degradation. The calculated binding energies (**Figure 2b**) indicate that TEP could stabilize PF_5 to inhibit HF formation, which is beneficial for the electrochemical cycling of LCO cathode at elevated temperature [21]. To verify this speculation, the elevated temperature storage property of various electrolytes was tested (**Figure S8**) and FED shows significant degradation due to HF formation.

The Li^+ solvation structure was studied by Fourier transform infrared spectroscopy (FTIR, **Figure S9**). The convoluted peaks around 1680~1880 cm^{-1} correspond to C=O stretching vibration of various solvents [22,23]. The quantitative analysis revealed that weakened coordination between the solvent and Li^+ upon the introduction of TEP and PS. Considering the potential detection limit of FTIR for trace additive effect, nuclear magnetic resonance (NMR) spectra were applied, which are more clearly reflect the changes in the local coordination environment. The downfield chemical shift of ^7Li observed in the NMR spectra (**Figure 2c**) indicates a weaker shielding effect around Li^+, hence implying the lowest Li^+ de-solvation for the FEDTP electrolyte. Next, the coordination state of was investigated by Raman spectroscopy (**Figure S10**). The increased relative intensity of solvated PF_6^- Raman peaks in both FEDT and FEDTP electrolytes suggests the formation of more CIPs [24]. With the gradual addition of TEP, a progressively increasing intensity of the Raman peak corresponding to solvated PF_6^- was observed, indicating that more PF_6^- ions coordinated with Li^+ (**Figure S11**). Together, the introduction of TEP solvent and PS additive effectively reduce the solvated number of carbonates so that PF_6^- anions tend to participate in the solvation shell. Furthermore, the addition of TEP solvent and PS additive further improves the ionic conductivity of the electrolyte, thereby facilitating faster Li^+ transport (**Figure S12**).

In order to elucidate the effect of TEP and PS for atom-level solvation sheath of Li^+, molecular dynamics (MD) simulation and density functional theoretical (DFT) calculation were carried out (**Figure S13**, **Figure S14** and **Figure S15**). In the FED electrolyte, EMC is the dominant solvent in the first Li^+ solvation shell at 25°C. With the addition of TEP solvent, the coordination numbers of original carbonates drop sharply due to the highest binding energy with Li^+ and the largest Van der

Waals volume of TEP molecules (**Figure S16** and **Figure S17**). Based on the statistical results in solvation shells, the average de-solvation energy of various electrolytes could be calculated using weighted average methods (**Figure S18**) [25]. It could be clearly observed that Li^+ de-solvation energy barrier decreased after the introduction of TEP, further substantiating the above spectroscopic results where more Li^+-PF_6^- CIPs were formed. Besides, the remarkable increase of CIPs is found in the FEDTP system and it could be largely attributed to the high affinity between PS and PF_6^- (**Figure S19**). When PS locates in the inner solvation sheath of Li^+ (**Figure S13**), it will induce more PF_6^- close to Li^+.

The temperature dependance of the Li^+ solvation structure also significantly influences the electrochemical performance at elevated temperature. Specifically, as the temperature increases from 25 to 45°C, intensified molecular thermal motion leads to a shift in solvation behavior: linear carbonates with higher binding energy (i.e., DEC) tend to enter the first solvation shell, whereas those with lower binding energy (i.e. EMC) exhibit a decrease in coordination number (**Figure 2d** and **Figure S15**). In contrast, TEP maintains a constant coordination number with Li^+ at both temperatures, demonstrating low temperature sensitivity, which is an advantageous property for systems subjected to thermal variations. As shown in **Figure 2e**, the vibration of P=O from free TEP is located at ~1270 cm^{-1} and solvated peak is located at ~1290 cm^{-1} [26,27]. With the rise of temperature, the characteristic peaks of TEP remained essentially unchanged, confirming the results of MD simulation.

Electrochemical performance under HV and elevated temperature

To highlight the significance of compatible electrolyte system under harsh conditions, the electrochemical performance of various electrolytes was examined in the voltage range of 3.0-4.6 V (vs. Li^+/Li) at 45°C. As shown in **Figure 3a**, FEDTP system enables the highest specific capacity of 190 mAh g^{-1} (corresponding to 90.4% capacity retention) than that cycled with other electrolytes after 200 cycles at 1 C, with an enhanced average coulombic efficiency (CE) of 99.86%. Even after 500 cycles, the battery still retains an 81.9% capacity retention rate. By comparing the capacity retention and mass loading delivered by FEDTP-LCO cells with those recently reported LCO batteries under HV and elevated temperatures (**Figure 3b**; see details listed in **Table S1**), this work exhibits state-of-the-art overall performance. In sharp contrast, the overpotentials of LCO electrodes

rapidly increased after cycling in FED or FEDT (**Figure S20**), inferring gradual interface deterioration and structural degradation of cathode materials. The cycling stability of LCO with the FEDP electrolyte (FED electrolyte with 1 vol% PS) was also evaluated, showing improved capacity retention rate compared with the FED system (**Figure S21**). The evolution of interfacial structure is confirmed by the Nyquist plots of half-cells after 200 cycles (**Figure 3c)**. The fitting results show that FEDTP displays significantly lower CEI impedance (R_{CEI}) as well as transfer resistance (R_{ct}) than other electrolytes. Combining the in-*situ* EIS of LCO cathodes during the 1st cycle (**Figure S22**), the R_{CEI} and R_{ct} remained stable under lithiation process in the FEDTP electrolyte, indicating the formation of a robust interphase with fast channels for Li^+.

Apart from the cycle life, FEDTP also facilitates superior rate capability over FED and FEDT (**Figure 3d** and **Figure S23**), with a capacity of 110 mAh g^{-1} at 8 C. To explore the origin of improved cycle stability, the diffusion coefficient of Li^+ (D_{Li}) in LCO cathode was calculated by the Randles-Sevcik equation according to the results of stepped sweep rate cyclic voltammetry (CV) (**Figure S24**) [28]. The D_{Li} values of lithiation and delithiation of LCO in FEDTP are measured to be 4.11×10^{-7} and 2.69×10^{-7} cm^2 s^{-1} respectively, about double those measured in FED (1.99×10^{-7} and 1.27×10^{-7} cm^2 s^{-1}). This finding well agrees with the 1st cycle CV curves of various electrolytes (**Figure S25**), where FEDTP exhibits the narrowest and most intense reversible redox peaks, suggesting faster charge transfer kinetics. To investigate the kinetics of Li^+ transfer across various CEIs, the activation energies of CEIs were calculated based on EIS at variable temperatures (**Figure S26** and **Figure S27**). Exhibiting the lowest activation energy (16.54 kJ mol^{-1}), the CEI derived from FEDTP exhibits the lowest energy barrier for Li^+ migration.

To further demonstrate the feasibility of our electrolyte design strategy under practical testing conditions, proof-of-concept LCO||graphite pouch cells (~1 Ah) were assembled and tested between 3.0 and 4.5 V under 45°C (**Figure 3e**). The cell cycled with FEDTP exhibited stable voltage profiles and voltage plateaus during cycling (**Figure S28**). After 150 cycles, FEDTP delivered suppressed rates of capacity fading (ΔQ_{FEDTP} = 0.1 Ah) as well as voltage decay (ΔV_{FEDTP} = 0.02 V) than FEDT (ΔQ_{FEDT} = 0.18 Ah, ΔV_{FEDT} = 0.04 V) and FED (ΔQ_{FED} = 0.33 Ah, ΔV_{FED} = 0.12 V), demonstrating huge potentials for practical applications. To exclude the potential impact of electrolytes on graphite negative electrodes, the electrochemical performance of Gr||Li half cells (**Figure S29**) were further researched and there was no significant difference between different electrolyte. It has been reported

that the significant thermal degradation of SEI layer and graphite anode starts at temperatures over 50℃ [29,30]. Therefore, the electrochemical performance of full cells at 45℃ was mainly dictated by the LCO cathode.

Structure stability of $LiCoO_2$

Generally, the structural instability of cathode materials originated from the surface. Herein, high angle annular dark field-scanning transmission electron microscopy (HAADF-STEM) and corresponding electron energy loss spectroscopy (EELS) measurements were performed to investigate the near-surface phase structure and the valence variations, respectively (**Figure 4a-f**). For LCO cycled in FED, a substantial near-surface region of spinel phase can be observed, capped by an outermost rock-salt (RS) phase approximately 5 nm thick. The above results suggest LCO underwent severe structural degradation in FED, primarily due to unrestricted surface side reaction. In contrast, LCO cycled in FEDT exhibited significantly milder degradation, with a much thinner RS phase (~2 nm) and a spinel phase (~5 nm) extending from the surface toward the bulk (**Figure 4b**). In stark contrast, the LCO maintains structural stability with minimal structural degradation (less than a 2 nm spinel phase on the surface) after 200 cycles in FEDTP (**Figure 4c**).

The near-surface structure of the cycled LCO is further identified by EELS (**Figure S30**). The crystal field splitting of Co-O octahedral configuration results in the generation of t_{2g} and e_g bands, corresponding to peak I at ~531.6 eV and bulge II at ~544 eV, respectively [31]. For LCO cycled in FED, the disappearance of pre-peak in O K-edge spectra at ~531.6 eV suggests the formation of lattice oxygen defects in the near-surface region due to the severe side reactions (**Figure 4d**). Besides, the shift (~1.4 eV) of Co L_3-edge peak to lower energy loss indicates that the surface Co^{3+} is reduced to $Co^{(3-x)+}$ and mixed phases (e.g., CoO and Co_3O_4) are formed, accompanying with Li^+ deficiency to accelerate structural degradation. For FEDT samples, the absence of pre-peak only exists in a limited area with a depth of 6 nm and a smaller shift (~1 eV) of Co L_3-edge peak is observed (**Figure 4e**), suggesting a less damaged surface structure. In comparison, for the LCO cycled in FEDTP, stable pre-peaks are detected in O K-edge spectra, while the location and intensity of Co L-edge peak maintain unchanged in the whole detected area (**Figure 4f**). It can be inferred from above results that the structural instability of LCO at 45℃ originates and propagates from the surface towards the bulk.

To reveal the evolution of surface TM-O bond vibration on the LCO cathode during cycling, in-

situ Raman spectra measurements were conducted (**Figure 4g**) for the 1st cycle [32]. The vibration peaks at ~500 and ~600 cm^{-1} correspond to the O-Co-O bending vibrations (E_g) and the Co-O symmetrical stretching (A_{1g}), respectively. During the reduction process, the intensity of vibration peaks attenuated significantly for LCO cathodes in FED and FEDT, suggesting the irreversible lithiation progress and destabilization of Co-O bonds. By contrast, the Raman spectra of the FEDTP group exhibit excellent reversibility of O-Co-O and Co-O bonds. Next, in-*situ* electrochemical mass spectrometry (DEMS) experiments were also conducted to analyze the evolution of CO_2 and O_2 in various electrolytes (**Figure S31**) [33]. For the FED electrolyte, the cell began to release CO_2 and O_2 at around 20% state of charge (SOC), corresponding to carbonate solvents decomposition and surficial lattice O loss. In sharp contrast, no obvious gas evolution was detected with the FEDTP electrolyte, suggesting that both carbonate solvents decomposition and oxygen loss were effectively suppressed. Besides, the X-ray absorption near-edge structure spectra at the K-edges of Co were collected after 200 cycles (**Figure 4h**). The absorption edge of Co for FEDTP shows a shift to higher energy, indicating the higher average valence states of Co element compared with that in FED and FEDT. It is consistent with the results of EELS and DEMS. Furthermore, the loss of active oxygen species is usually accompanied by dissolution of low-valence TM ions. Both XPS and inductively coupled plasma atomic emission spectroscopy (ICP-AES) results of cycled Li anode surface with different electrolytes confirmed a large amount of Co^{2+} dissolved and shuttled to Li in FED (**Figure S32** and **Figure S33**), which can be mitigated in both FEDT and FEDTP. Besides, the lattice parameters *a* and *c* calculated by XRD data for LCO cathode cycled in the FEDTP electrolyte deviate less from the pristine LCO than those in other electrolytes (**Figure S34** and **Figure S35**), indicating the improved reversibility of the bulk structure. From above results, it can be concluded that our electrolyte design strategy stabilizes the crystal structure of LCO at the (near-)surface by suppressing lattice O loss, Co dissolution as well as violent decomposition of the electrolyte.

Constructing robust cathode electrolyte interphase

Different from the results obtained at 45°C, the galvanostatic cycling of LCO cathodes with FED, FEDT and FEDTP electrolytes at 25°C exhibited very similar capacity retention rates (**Figure S36**). Next, X-ray photoelectron spectroscopy (XPS) was employed to reveal the compositional evolution of CEI. At 25°C, the CEI components formed in all three electrolytes are very similar, except that

peaks at ~133 eV and ~168 eV can be observed after the introduction of TEP and PS, respectively, suggesting the formation of Li_3PO_4 and Li_2SO_3 (**Figure 5a**). This result well agrees with the cycling performance of three electrolytes at room temperature.

However, at 45°C, the chemical composition of CEI layer in FED has changed dramatically (**Figure 5b**), while the CEI evolution in FEDTP is barely changed under elevated temperature operation. The F 1s spectra show that the high LiF content in FEDTP is well preserved, without showing the increasing amount of undesirable decomposition species of $LiPF_6$ (e.g. Li_xPF_z, $Li_xPO_yF_z$) in other two electrolytes, especially FED. The appearance of C-F bonds (corresponding to the polyvinylidene fluoride binder) also indicates that the CEI formed on LCO in FED completely fails at 45°C, resulting in a large amount of exposed electrode surface. This result is well corroborated by the O 1s spectra, where a significant Co-O peak (~529 eV) could be observed in FED, indicating the exposed LCO particles. When compared with FED, FEDT effectively reduced the Co-O peak whereas the FEDTP-derived CEI managed to protect the cathode after 200 cycles at 45°C. From the P 2p and S 2p spectra, it can be observed both Li_3PO_4 and Li_2SO_3 components remain stable at 200 cycles at 45°C, well agreeing with calculation results. The CEI components formed in initial cycling stage (3 cycles) of various electrolytes at 45°C were also examined by XPS (**Figure S37**). The initial CEI formed by all electrolytes at 45°C exhibits a composition similar to that shown in **Figure 5a**, indicating that the CEI structure remains relatively intact at this stage. However, during prolonged cycling, the CEI generated in FED degraded rapidly, whereas the stepwise introduction of TEP and PS sequentially facilitated the formation of heat-tolerant Li_3PO_4 and adhesive Li_2SO_3, thereby ensuring that the CEI maintains its morphological and compositional stability at elevated temperatures.

Furthermore, in-*situ* FTIR was performed to reveal the interfacial evolution of various electrolytes during CEI formation (see the schematic setup in **Figure S38**). Surface-enhanced in-*situ* FTIR spectra (**Figure S39**) show that during the charge process from OCV to 4.6 V, the stepwise addition of TEP and PS significantly inhibited carbonate decomposition, as evidenced by the diminished reverse peak intensities of FEC (~1830 cm^{-1}), Li^+-FEC (~1800 cm^{-1}), EMC/DEC (~1742 cm^{-1}) and Li^+-EMC/DEC (~1708 cm^{-1}) peaks. Subsequently, the oxidation pathways of TEP and PS were further investigated via DFT calculations (**Figure S40**). Upon electron loss, both TEP and PS exhibit a tendency to cleave the C-O bond. Based on the above experimental results and theoretical analysis,

detailed decomposition pathways of TEP and PS are proposed (**Figure S41**). The decomposition of TEP leads to the formation of Li_3PO_4 and ethylene, while PS decomposes into Li_2SO_3 and organosulfite species such as RSO_3Li. Given their structural similarity to Li_2SO_3, the minor organosulfite species (RSO_3Li) are reasonably expected to possess adhesion characteristics. The detection of ethylene signal in DEMS test and Li_3PO_4 signal in XPS test (using $LiClO_4$ as Li-salt) further confirm the decomposition path of TEP (**Figure S42**).

To reveal the spatial distribution of various chemical components within the CEI, time of flight secondary-ion mass spectrometry (TOF-SIMS) was performed on cycled LCO electrodes (**Figure S43** and **Figure 5c**). For FEDTP, it could be observed that after long cycling, the cathode is covered by a stable CEI composed of LiF_2^-, PO_3^- and SO_3^- fragments. In addition, the S 2p XPS results after etching (**Figure S44**) show that Li_2SO_3 is primarily located in the outermost layer of the CEI. By combining XPS with TOF-SIMS results, it is concluded that Li_3PO_4, LiF and Li_2SO_3 formed in FEDTP are predominantly distributed in the inner, middle, and outer regions of the CEI, respectively [34,35]. This trilayered CEI structure aligns well with the design concept illustrated in **Figure 1**, where the inner Li_3PO_4 stabilizes the surficial oxygen of LCO cathode, while the outer Li_2SO_3 firmly adheres to LCO and other CEI inorganics, forming a compact protective cap that effectively suppresses the dissolution of the entire CEI layer.

Furthermore, the significantly weaker intensity of C_2HO^- in FEDTP demonstrated the suppressed decomposition of carbonate solvent. In contrast, a large number of POF_2^- and $PO_2F_2^-$ fragments were detected on the LCO surface in FED, suggesting the excessive decomposition of $LiPF_6$. The broken distribution of LiF_2^- was deduced to relate to the instability of CEI under 45°C that causes dissolution of organic species, hence the detachment of LiF. After the addition of TEP, more distinctive LiF_2^- fragments could be observed on the LCO surface, accompanied by PO_2^- and PO_3^- species, indicating the partial dissolution of CEI layer. However, the widespread presence of carbonate decomposition products (C_2HO^- species) still indicates that the interface of LCO is not effectively passivated. Besides, the CoF_3^- fragments are the dissolved products of Co attacked by electrolyte, while the CoO_2^- fragments are considered as an indication of LCO cathode materials. Due to the effective retention of CoO_2^- components (**Figure S45**) and the minimal presence of CoF_3^- components, this result further confirms that FEDTP can effectively suppress side reactions between the electrolyte and LCO [36,37].

The thermal stability of CEI layer was further investigated through the electrochemical characterization and differential scanning calorimetry (DSC) measurement. At 45°C, by allowing the half-charged cells to rest for 24 hours, the cells with FED and FEDT electrolytes exhibited noticeable potential drops, indicating continuous dissolution of the CEI (**Figure 6a**). In sharp contrast, the cell with FEDTP exhibited minimal potential drop, showing that the CEI remains stable and is not readily dissolved, even under prolonged elevated temperature storage. The floating charge test was also conducted to evaluate the side reactions between the fully charged cathode and electrolyte (**Figure S46)**. Compared with the FED and FEDT electrolytes, LCO cycling in the FEDTP electrolyte exhibited significantly lower leakage currents throughout the entire floating period (100 h), indicating reduced parasitic reactions and enhanced electrochemical stability. As shown in **Figure 6b**, the total heat-releasing of LCO cycling in FEDTP electrolyte (~631 J g^{-1}) is lowest compared with that of LCO cycling in the FED electrolyte (~5149 J g^{-1}) and FEDT electrolyte (~1335 J g^{-1}), suggesting the most compact and inorganics-rich CEI layer formed in the FEDTP electrolyte. Moreover, the decomposition temperature of CEI formed in FEDTP was delayed to ~483℃, indicating an enhanced thermal stability of CEI layer.

Then, the microstructure of CEI formed in different electrolytes was studied by cryo-transmission electron microscopy (cryo-TEM). After cycling in the FED electrolyte at HV and 45°C, a broken and thick surface layer was observed on LCO cathode which cannot provide the effective protection for electrode (**Figure 6c**). In sharp contrast, the use of TEP solvent and PS additive results in a thin and uniform CEI layer that passivates the LCO surface without compromising Li^+ transfer. Combing with the results of scanning electron microscopy (SEM), the obvious dissolution of CEI was found in the FED and FEDT electrolyte (**Figure S47**), exposing the highly active Co on the cathode surface and inducing repeated electrolyte consumption. Next, atomic force microscope (AFM) was applied to characterize the roughness and mechanical properties of CEI layers on LCO surface with various electrolytes (**Figure 6d**, **Figure S48** and **Figure S49**). The LCO particle cycled in FEDTP shows a more uniform and smoother surface morphology compared to that cycled in the FED and FEDT electrolytes, which is consistent with the results of SEM and cryo-TEM. After logarithm transformation of the Derjaguin-Muller-Toporov (DMT) modulus, the CEI formed in FEDTP exhibits a more uniform distribution with a higher average value (9.74 Log(Pa)) compared with those formed in FED (9.25 Log(Pa)) and FEDT (9.35 Log(Pa)), manifesting a denser inorganics-rich CEI

layer. In contrast, CEI layer rich in organic components with damaged structures naturally displays poorer mechanical properties.

Revealed the improving mechanism of $LiCoO_2$

As shown in **Figure S50**, the CEI formed in the FED system primarily consists of LiF and RPO_2F_2, which can disintegrate (e.g., through decomposition and dissolution in the electrolyte) under elevated temperature and high-voltage conditions, resulting in an incoherent distribution. To address the limitations of a single inorganic component, two additional inorganic species with excellent thermal stability (Li_3PO_4 and Li_2SO_3) were introduced into the CEI. On one hand, the addition of TEP helps inhibit HF formation and generates inorganic Li_3PO_4, which stabilizes the interfacial lattice oxygen of the LCO cathode *via* PO_4^{3-} and accelerates Li^+ transport across the CEI. On the other hand, the strong adhesion of Li_2SO_3 effectively anchors other CEI components to the LCO surface. The combination of these three components and their spatial distribution achieves a breakthrough in the densification of the CEI, which effectively passivates the high-activity sites on the cathode surface under high-voltage conditions and prevents the dissolution of organic materials at elevated temperatures. Thus, the heterogeneous inorganics comprising the dense CEI enhance interfacial stability at elevated temperatures and improve the electrochemical performance of the HV-LCO cathode.

CONCLUSION

In summary, through introducing TEP and PS into the electrolyte, a trilayered CEI, comprising Li_3PO_4, LiF, and Li_2SO_3, which arranged hierarchically from the innermost to the outermost layer, is constructed for high-voltage cathode at elevated temperature. We systematically integrated the synergistic effects of multiple inorganic CEI components through well-established additives. The electrochemically tailored interphase rich in LiF, Li_3PO_4, and Li_2SO_3 inorganic components could not only restricts the excessive oxidation decomposition of electrolyte, but also passivates the Co^{2+} catalytic sites and restrain the TM dissolution. The designed CEI exhibits the favorable thermal stability and adhesion force which protects the structural integrity of LCO cathode under severe conditions. Furthermore, the modified CEI layer markedly improves the charge transfer kinetics and the commercial pouch cells (1 Ah) could achieve the impressive cycling performance. The proposed

design strategy of CEI greatly expands the application fields of LCO cathode and is suitable for other cathode materials.

ACKNOWLEDGEMENTS

The authors thank the support from the BL11B station in the Shanghai Synchrotron Radiation Facility.

FUNDING

This work was supported by the National Natural Science Foundation of China (92472206), the Major Science and Technology Infrastructure Project of Material Genome Big-science Facilities Platform supported by Municipal Development and Reform Commission of Shenzhen, International joint Research Center for Electric Vehicle Power Battery and Materials (2015B01015), THE Guangdong Key Laboratory of Design and calculation of New Energy Materials (2017B030301013), and the Shenzhen Key Laboratory of New Energy Resources Genome Preparation and Testing (ZDSYS201707281026184).

AUTHOR CONTRIBUTIONS

Shiming Chen: Electrolyte design, Electrochemical measurements, Theoretical calculation, Formal analysis and Writing-original draft; Wenguang Zhao: Characterization resources, Formal analysis and Writing-original draft; Guorui Zheng: Electrolyte design and Writing-review & editing; Chenyu Yang: Characterization resources; Taowen Chen: Theoretical calculation; Hengyu Ren: Characterization resources; Yue Zuo: Characterization resources; Xiangming Yao: Characterization resources; Ke Li: Characterization resources; Haoyu Xue: Characterization resources; Jianjun Fang: Electrochemical measurements; Yuxiang Huang: Investigation; Kai Yang: Visualization; Zu-Wei Yin: Characterization resources; Luyi Yang: Project administration, Funding acquisition and Writing-review & editing; Feng Pan: Project administration, Funding acquisition and Writing-review & editing. All authors participated in the discussion of the results and contributed to the data analyses.

Conflict of interest statement. None declared.

REFERENCES

[1] Wang L, Chen B, Ma J *et al*. Reviving lithium cobalt oxide-based lithium secondary batteries-toward a higher energy density. *Chem Soc Rev* 2018; 47: 6505–602.

[2] Wu F, Maier J, Yu Y. Guidelines and trends for next-generation rechargeable lithium and lithium-ion batteries. *Chem Soc Rev* 2020; 49: 1569–614.

[3] Lin C, Li J, Yin ZW *et al.* Structural understanding for high-voltage stabilization of lithium cobalt oxide. *Adv Mater* 2024; 36: 2307404.

[4] Sun Z, Zhao J, Zhu M *et al.* Critical problems and modification strategies of realizing high-voltage $LiCoO_2$ cathode from electrolyte engineering. *Adv Energy Mater* 2024; 14: 2303498.

[5] Zheng WC, Shi CG, Dai P *et al.* A functional electrolyte additive enabling robust interphases in high-voltage Li‖$LiNi_{0.8}Co_{0.1}Mn_{0.1}O_2$ batteries at elevated temperatures. *J Mater Chem A* 2022; 10: 21912–22.

[6] Zhang A, Yang E, Bi Z *et al.* Unlocking 4.7 V $LiCoO_2$ with a counterintuitive low-concentration fluoroborate dual-salt electrolyte by anion-derived interfacial chemistry. *ACS Energy Lett* 2025; 10: 1245–54.

[7] Ji Y, Huang Y, Dong Z *et al.* Anion adsorption at the inner-helmholtz plane directs cathode electrolyte interphase formation. *Angew Chemie Int Ed* 2025; 202425535.

[8] Fan X, Ji X, Han F *et al.* Fluorinated solid electrolyte interphase enables highly reversible solid-state Li metal battery. *Sci Adv* 2018; 4: aau9245.

[9] Yang X, Wang C, Yan P *et al.* Pushing lithium cobalt oxides to 4.7 V by lattice-matched interfacial engineering. *Adv Energy Mater* 2022; 12: 2200197.

[10] Ren H, Zheng G, Li Y *et al.* Stabilizing $LiCoO_2$ at 4.6 V by regulating anti-oxidative solvents. *Energy Environ Sci* 2024; 17: 7944–57.

[11] Wu J, Wu Y, Wang L *et al.* Challenges and advances in rechargeable batteries for extreme-condition applications. *Adv Mater* 2024; 36: 2308193.

[12] Sun Z, Li F, Ding J *et al.* High-voltage and high-temperature $LiCoO_2$ operation via the electrolyte additive of electron-defect boron compounds. *ACS Energy Lett* 2023; 8: 2478–87.

[13] Li Y, Wen B, Li N *et al.* Electrolyte engineering to construct robust interphase with high ionic conductivity for wide temperature range lithium metal batteries. *Angew Chemie Int Ed* 2025; 64: e202414636.

[14] Wu D, Zhu C, Wang H *et al.* Mechanically and thermally stable cathode electrolyte interphase enables high-temperature, high-voltage Li||$LiCoO_2$ batteries. *Angew Chemie Int Ed* 2024; 63: e202315608.

[15] Li S, Yang K, Quan Y *et al.* Precycling strategy in suitable voltage to improve the stability of interfacial film and suppress the decline of $LiNi_{0.6}Mn_{0.2}Co_{0.2}O_2$ cathode at elevated temperatures. *ACS Appl Mater Interfaces* 2024; 16: 26245–56.

[16] Chen Y, He Q, Mo Y *et al.* Engineering an insoluble cathode electrolyte interphase enabling high performance NCM811||graphite pouch cell at 60°C. *Adv Energy Mater* 2022; 12: 2201631.

[17] Jayasree SS, Murali AS, Nair S *et al.* Recent progress on the low and high temperature performance of nanoscale engineered Li-ion battery cathode materials. *Nanotechnology* 2022; 33: 352001.

[18] Wu Z, Zeng G, Yin J *et al.* Unveiling the evolution of $LiCoO_2$ beyond 4.6 V. *ACS Energy Lett* 2023; 8: 4806–17.

[19] Lv L, Zhang H, Lu D *et al.* Additive engineering enables aggressive high-voltage $LiCoO_2$ lithium-ion batteries. *Joule* 2025; 9: 101846.

[20] Chen X, Bai YK, Zhao CZ *et al.* Lithium bonds in lithium batteries. *Angew Chemie Int Ed* 2020; 59: 11192–5.

[21] Fang W, Wen Z, Wang F *et al.* Triple-function eutectic solvent additive for high performance lithium metal batteries. *Sci Bull* 2024; 69: 1686–96.

[22] Zou Y, Liu G, Wang Y *et al.* Intermolecular interactions mediated nonflammable electrolyte for high-voltage lithium metal batteries in wide temperature. *Adv Energy Mater* 2023; 13: 2300443.

[23] Chen Y, He Q, Zhao Y *et al.* Breaking solvation dominance of ethylene carbonate via molecular charge engineering enables lower temperature battery. *Nat Commun* 2023; 14: 8326.

[24] Song G, Yi Z, Su F *et al.* Boosting the low-temperature performance for Li-ion batteries in $LiPF_6$-based local high-concentration electrolyte. *ACS Energy Lett* 2023; 8: 1336–43.

[25] Ji H, Wang Z, Sun Y *et al.* Weakening Li^+ de-solvation barrier for cryogenic Li-S pouch cells. *Adv Mater* 2023; 35: 2208590.

[26] Liu S, Mao J, Zhang Q *et al.* An intrinsically non-flammable electrolyte for high-performance

potassium batteries. *Angew Chemie Int Ed* 2020; 59: 3638–44.

[27] Guo Q, Cai Y, Chen L *et al.* Competitive solvation chemistry modulated nonflammable pseudo ultralow concentration electrolyte toward high-voltage li metal batteries. *Adv Funct Mater* 2025; 2500500.

[28] Ren X, Zhao Q, McCulloch WD *et al.* MoS_2 as a long-life host material for potassium ion intercalation. *Nano Res* 2017; 10: 1313–21.

[29] Hölderle T, Monchak M, Baran V *et al.* Thermal structural behavior of electrochemically lithiated graphite (Li_xC_6) anodes in Li-ion batteries. *Batter Supercaps* 2024; 7: e202300499.

[30] Wu J, Weng S, Zhang X *et al.* In situ detecting thermal stability of solid electrolyte interphase (SEI). *Small* 2023; 19: 2208239.

[31] Qi S, Guan Y, Wang J *et al.* A pre-fatigue training strategy to stabilize $LiCoO_2$ at high voltage. *Energy Environ Sci* 2024; 17: 2269-78.

[32] Zhang F, Qin N, Li Y *et al.* Phytate lithium as a multifunctional additive stabilizes $LiCoO_2$ to 4.6 V. *Energy Environ Sci* 2023; 16: 4345–55.

[33] Yoon M, Dong Y, Yoo Y *et al.* Unveiling nickel chemistry in stabilizing high-voltage cobalt-rich cathodes for lithium-ion batteries. *Adv Funct Mater* 2020; 30: 1907903.

[34] Yuan X, Dong T, Liu J *et al.* Bi-affinity electrolyte optimizing high-voltage lithium-rich manganese oxide battery via interface modulation strategy. *Angew Chemie Int Ed* 2023; 62: e202304121.

[35] Wu L, Yuan H, An Y *et al.* Sulfurized composite interphase enables a highly reversible zn anode. *Angew Chemie Int Ed* 2025; 64: e202419495.

[36] Tan X, Zhang Y, Xu S *et al.* High-entropy surface complex stabilized $LiCoO_2$ cathode. *Adv Energy Mater* 2023; 13: 2300147.

[37] Tan X, Zhao T, Song L *et al.* Simultaneous near-surface trace doping and surface modifications by gas-solid reactions during one-pot synthesis enable stable high-voltage performance of $LiCoO_2$. *Adv Energy Mater* 2022; 12: 2200008.

[38] Jain A, Ong SP, Hautier G *et al.* Commentary: the materials project: a materials genome approach to accelerating materials innovation. *APL Mater* 2013; 1: 011002.

[39] Munro JM, Latimer K, Horton MK *et al.* An improved symmetry-based approach to reciprocal space path selection in band structure calculations. *Npj Comput Mater* 2020; 6: 112.

[40] Du YA, Holzwarth NAW. Li ion diffusion mechanisms in the crystalline electrolyte γ-Li_3PO_4. *J Electrochem Soc* 2007; 154: A999.

[41] Bai S, Bao W, Qian K *et al.* Elucidating the role of prelithiation in Si-based anodes for interface stabilization. *Adv Energy Mater* 2023; 13: 2301041.

[42] Zhang J, Zhang H, Weng S *et al.* Multifunctional solvent molecule design enables high-voltage Li-ion batteries. *Nat Commun* 2023; 14: 2211.

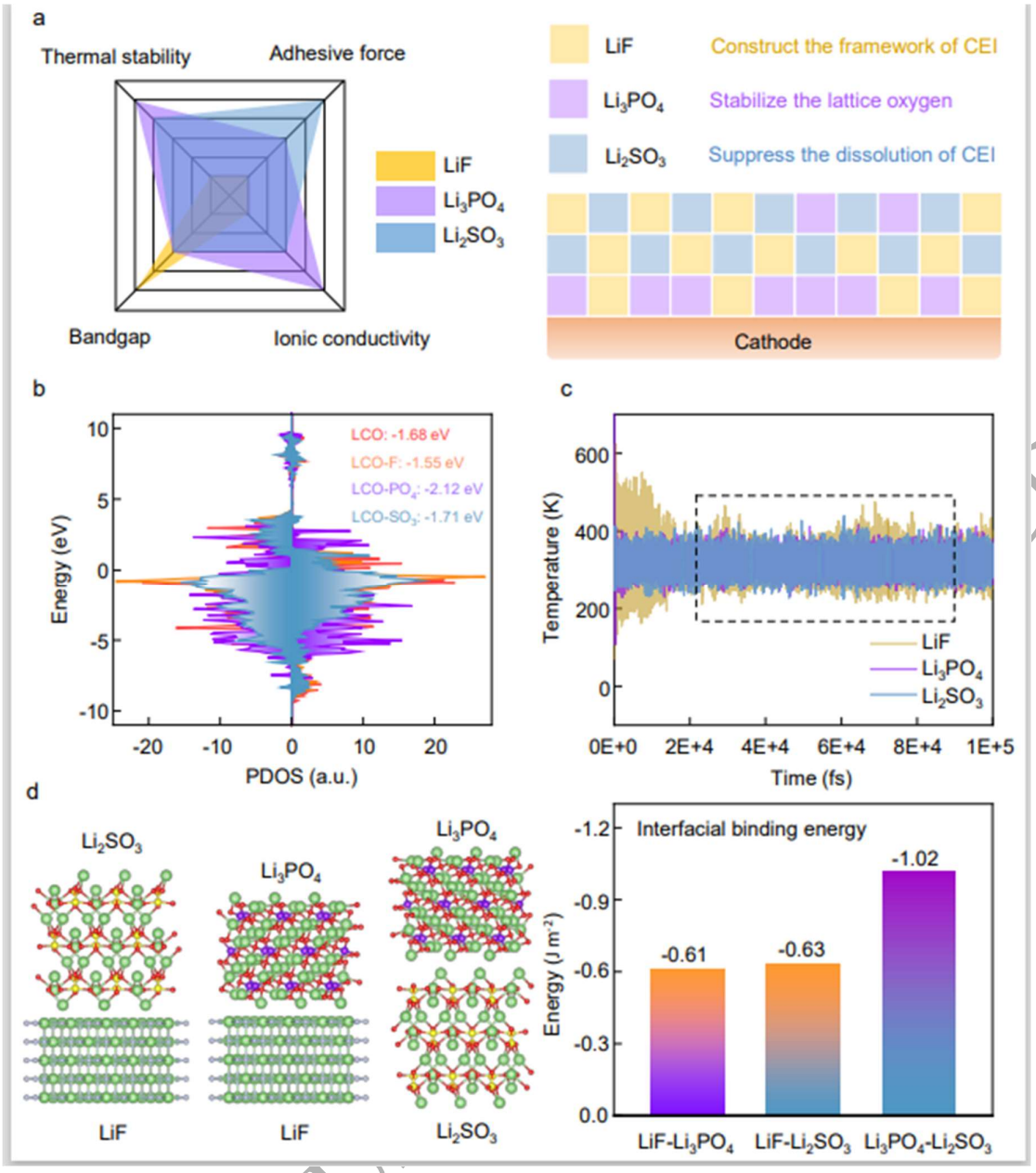

Figure 1. (a) Radar charts of three inorganic components and schematic illustration of CEI design. The bandgap and ionic conductivity data are collected from the previous research and material database [38–42]; (b) Calculated density of states of O 2p for the outermost single layer of cobalt-oxygen in LCO with various functional groups; (c) Temperature curves of LiF, Li_3PO_4 and Li_2SO_3 in AIMD calculation at 45°C (the more curve fluctuation corresponding the more unstable component); (d) Interfacial binding energies between the LiF (100), Li_3PO_4 (101) and Li_2SO_3 (010).

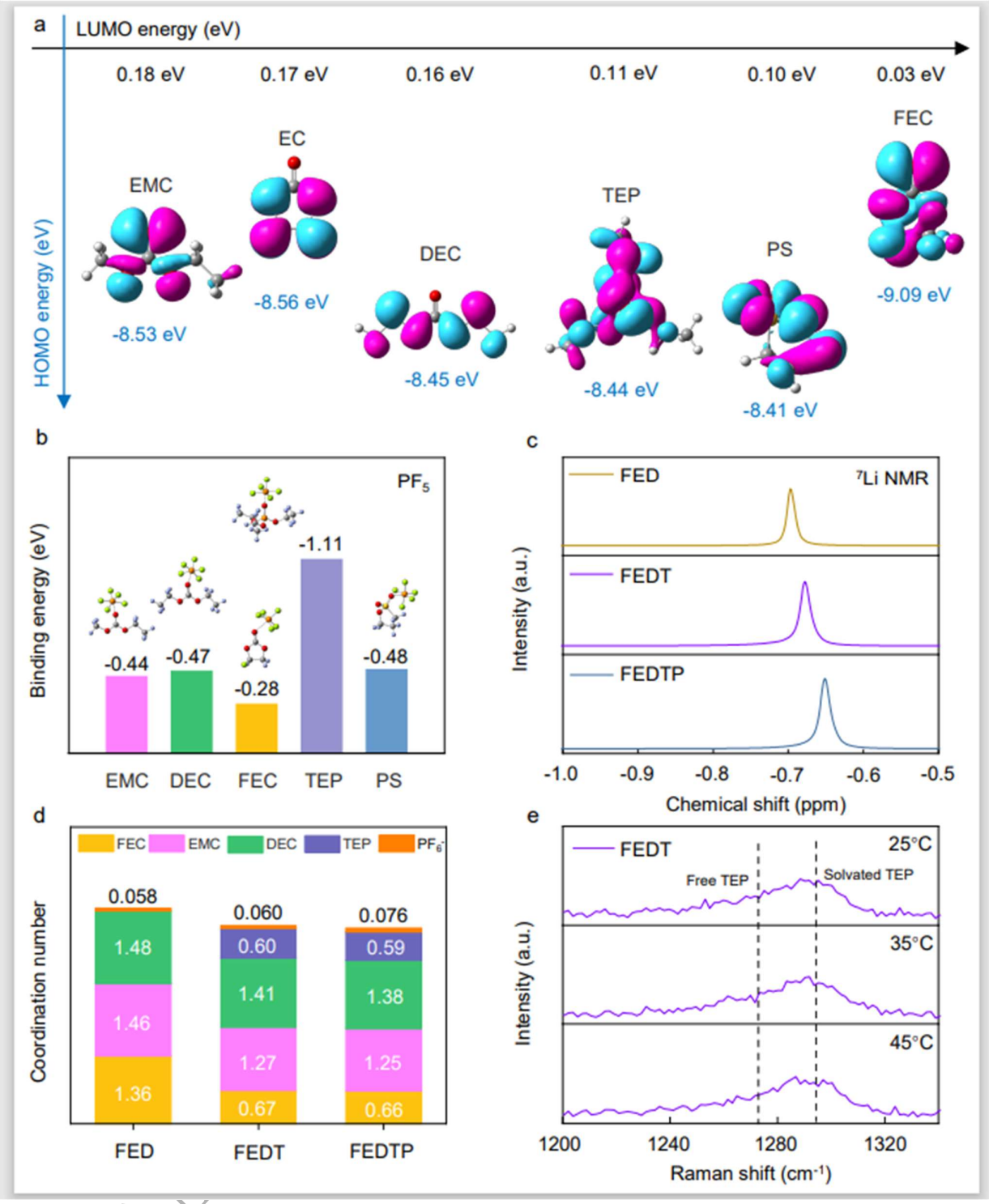

Figure 2. (a) Diagram of calculated HOMO/LUMO energies of electrolyte molecules; (b) Binding energies of electrolyte molecules with PF_5; (c) ^7Li NMR spectra of various electrolytes at 25°C; (d) Coordination environment of Li^+ in various electrolytes at 45°C according to the molecular dynamics simulation; (e) Raman spectra of FEDT electrolyte at various temperatures.

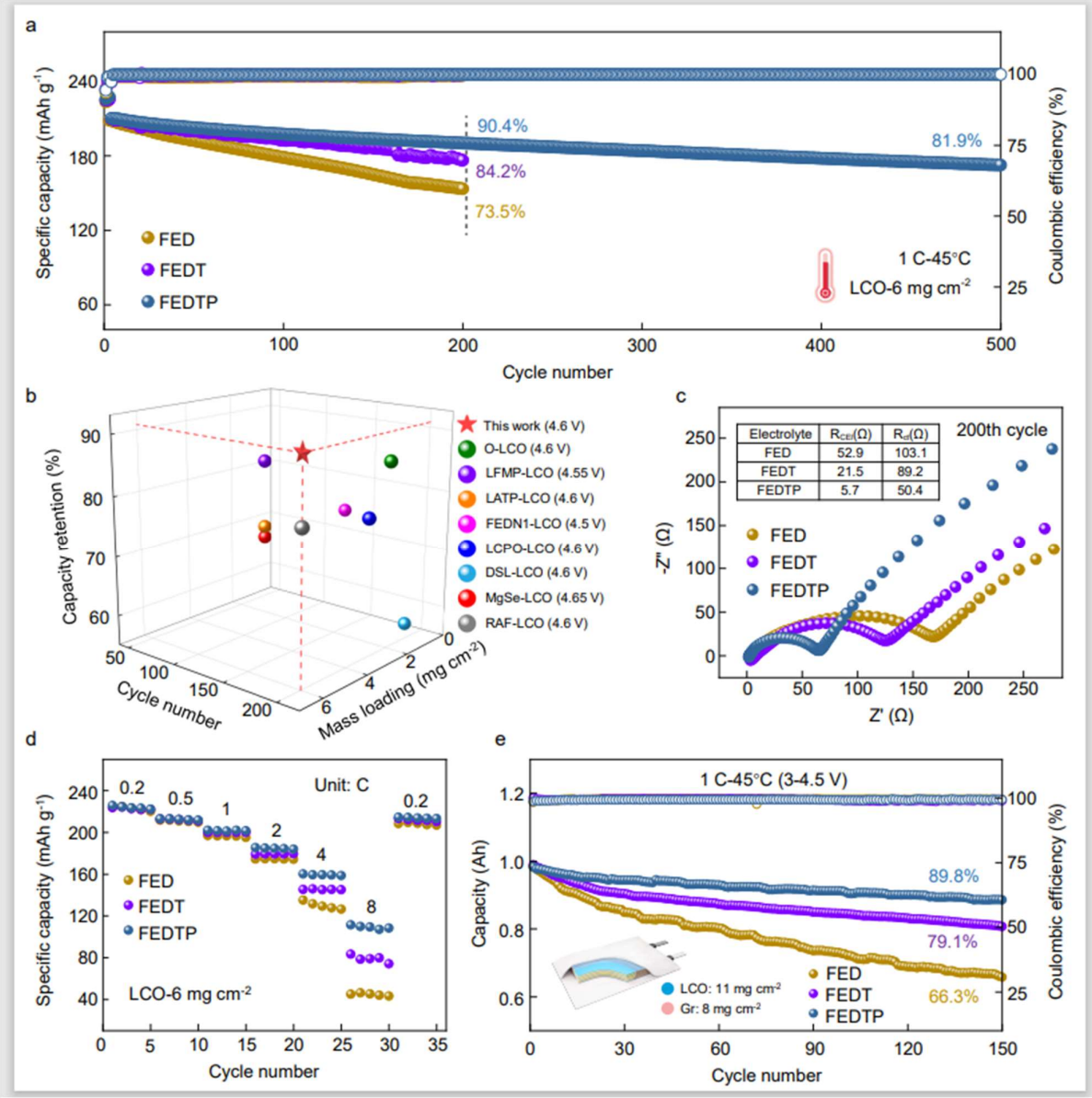

Figure 3. (a) Galvanostatic cycling performance and coulombic efficiency of LCO cathodes with various electrolytes at a rate of 0.2 C for the first 3 cycles and 1C for the subsequent cycles; (b) Comparison of the LCO electrochemical performance under elevated temperature condition; (c) EIS of LCO cathodes with various electrolytes after 200 cycles; (d) Rate performance of LCO cathodes with various electrolytes; (e) Galvanostatic cycling performance and coulombic efficiency of pouch cells at a rate of 1 C with various electrolytes.

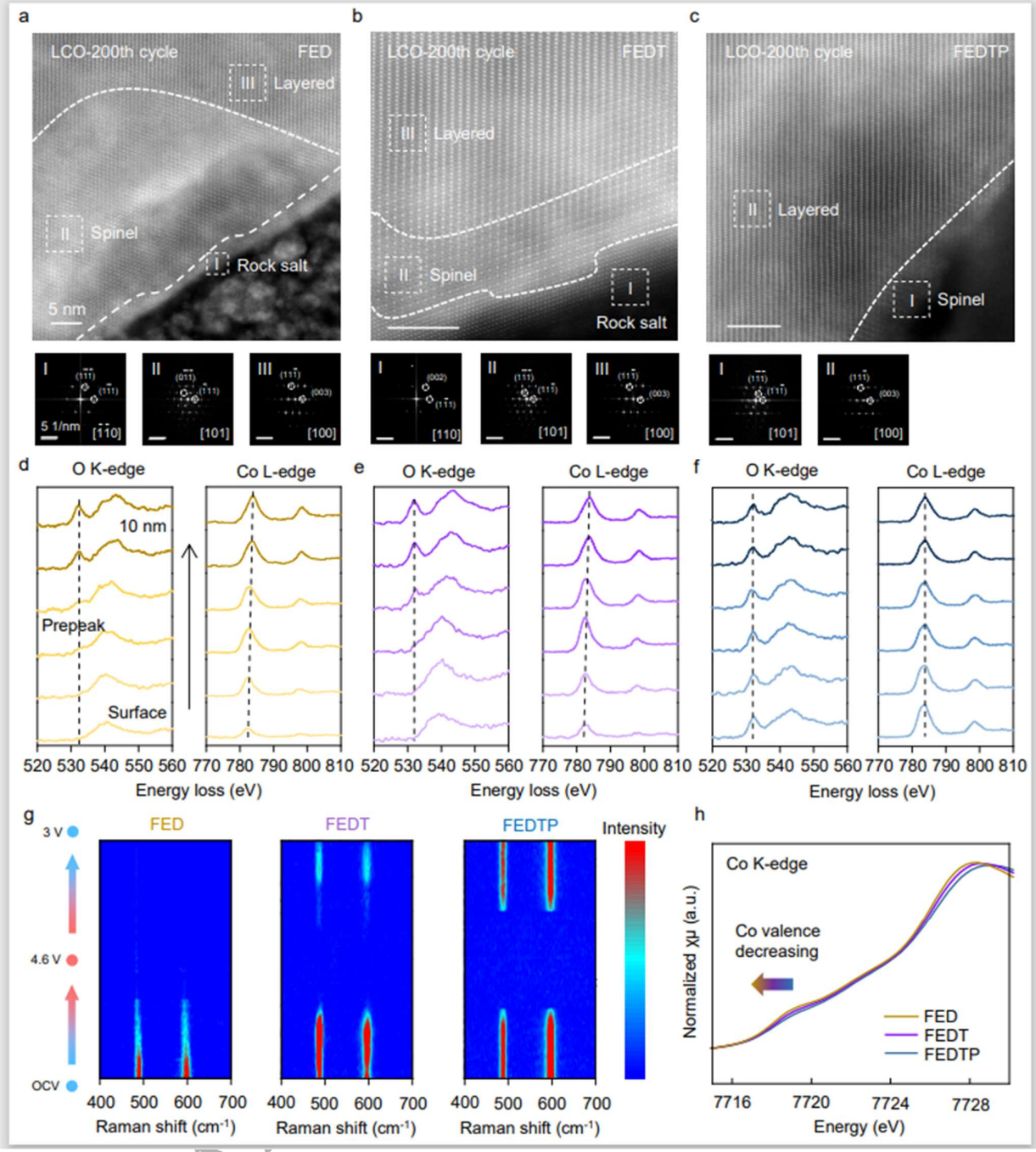

Figure 4. HAADF-STEM images of LCO cathodes with FED (a), FEDT (b) and FEDTP (c) electrolytes after 200 cycles at 45°C; Fast Fourier Transform (FFT) diffraction fringes corresponding to the marked areas in each TEM image are shown below the respective images; EELS spectra in the surface region of LCO cathodes with FED (d), FEDT (e) and FEDTP (f) electrolytes after 200 cycles at 45°C; (g) In-*situ* Raman spectra of LCO cathodes with various electrolytes in the first cycle at 45°C; (h) Co K-edge XANES spectra of LCO cathodes after 200 cycles at 45°C with various electrolytes.

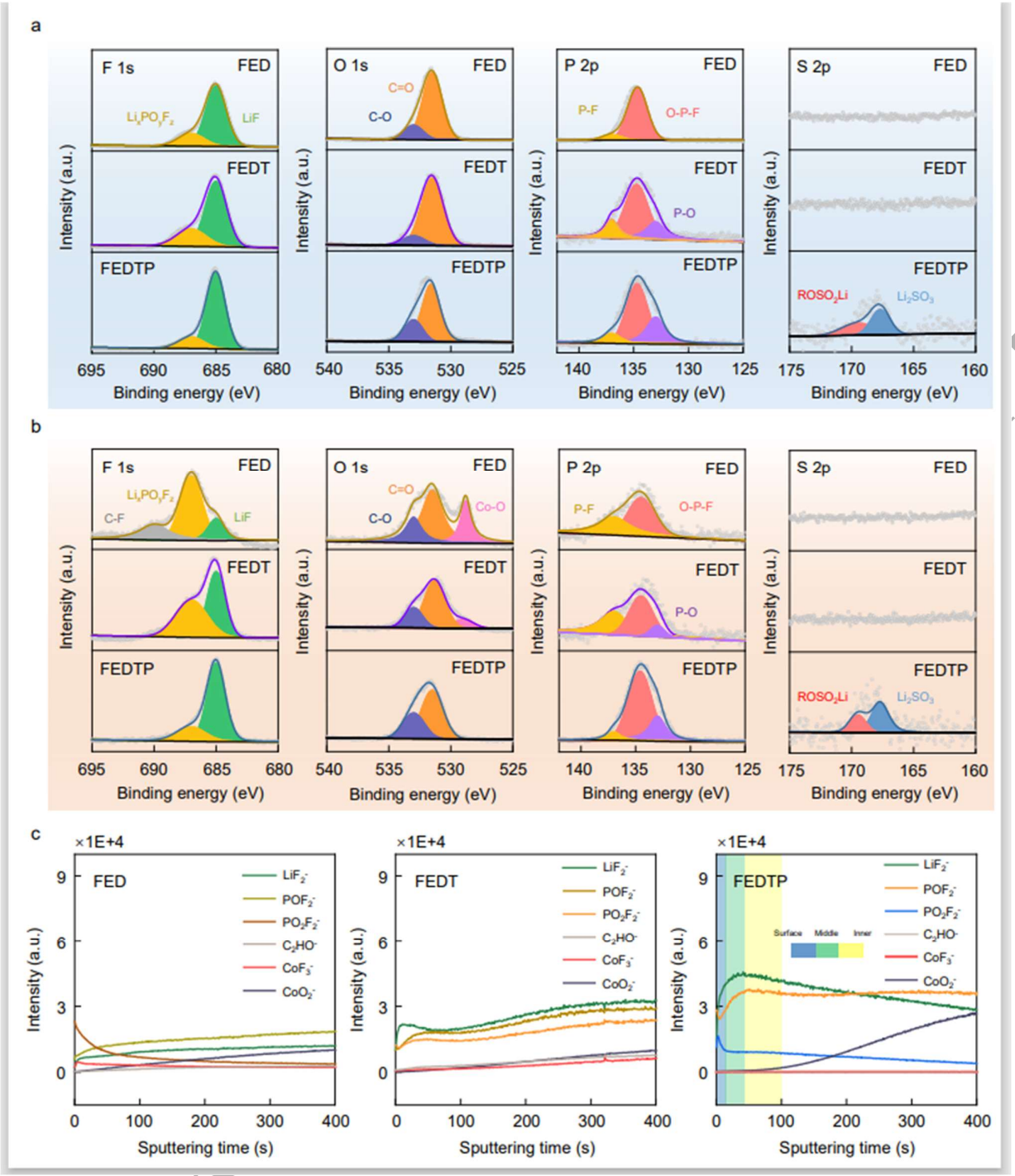

Figure 5. F 1s, O 1s, P 2p and S 2p X-ray photoelectron spectroscopy (XPS) spectra of LCO cathodes with various electrolytes after 200 cycles at 25°C (a) or 45°C (b); (c) Depth profiles of various secondary ion fragments during the TOF-SIMS measurement for LCO cathodes with various electrolytes after 200 cycles at 45°C.

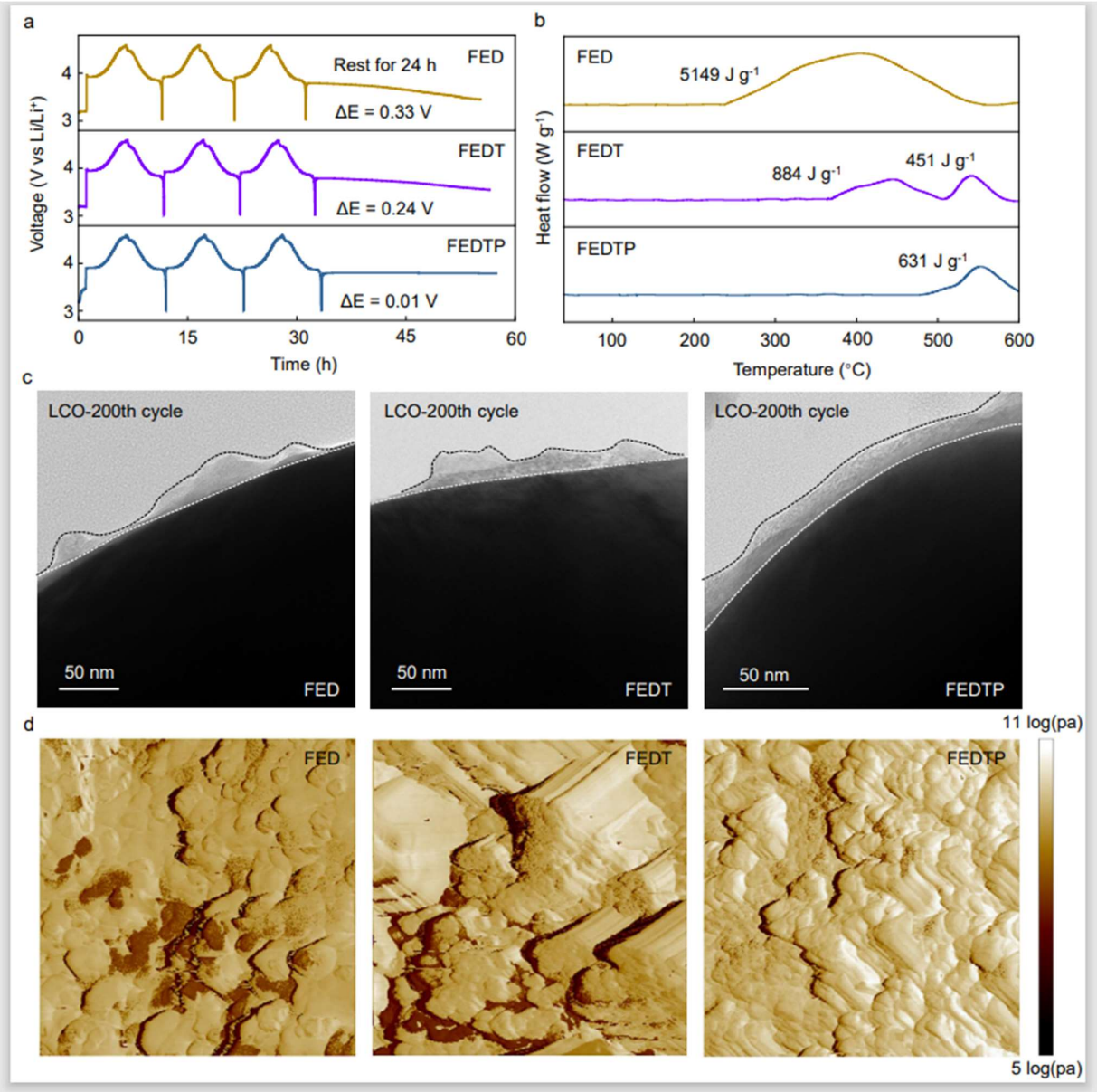

Figure 6. (a) Time-voltage curves of LCO cathodes with various electrolytes under 0.2 C current density at 45°C; (b) DSC curves of LCO cathodes under lithiation state with various electrolytes after 200 cycles at 45°C; (c) Cryo-TEM images of LCO cathodes with FED, FEDT and FEDTP electrolytes after 200 cycles at 45°C; (d) Mechanical property of CEI on the LCO cathodes with FED, FEDT and FEDTP electrolytes after 200 cycles at 45°C measured *via* AFM (2 μm × 2 μm).